Multiphase flow and granular mechanics

Invited Articles

Multiphase flow and granular mechanics

Ruben Juanes,* Yue Meng, and Bauyrzhan K. Primkulov
Massachusetts Institute of Technology, 77 Massachusetts Avenue, Cambridge, Massachusetts 02139, USA

(Received 21 August 2020; accepted 7 October 2020; published 24 November 2020)

In this perspective we provide a brief overview of the state of knowledge and recent progress in the area of multiphase flow through deformable granular media. We show, with many examples, that the interplay between viscous, capillary, and frictional forces at the pore scale determines the mode of fluid invasion. We pay particular attention to the central role of wettability on the morphology of granular-pack deformation and failure. Beyond their intrinsic interest as processes that give rise to spectacular pattern formation, these coupled phenomena in granular media can control continental-scale fluxes like methane venting from the seafloor and geohazards like earthquakes and landslides. We conclude this perspective by pointing to fundamental knowledge gaps and exciting avenues of research.

DOI: 10.1103/PhysRevFluids.5.110516

I. INTRODUCTION

The flow of multiple fluid phases through permeable media is key to the understanding, prediction, and design of environmental systems, energy resources, climate-change mitigation strategies, and industrial processes. Examples include infiltration of water into the vadose zone [1–4] and resilience of water-limited ecosystems [5–7], contamination (and subsequent remediation) of underground bodies of water by nonaqueous phase liquids [8,9], geologic CO_2 storage [10–15], hydrocarbon recovery from conventional [16,17] and unconventional formations [18], methane venting from organic-rich sediments in lakes and the seafloor [19–21], formation and dissociation of methane hydrates in permafrost regions and in ocean sediments [22], water dropout in low-temperature polymer-electrolyte fuel cells [23,24], and microfluidics towards laboratory-on-a-chip technology [25–33].

The interplay between multiphase flow and granular mechanics controls the morphological patterns, evolution, and function of a wide range of systems. For example, it determines the self-assembly of particles and patterning of substrates at the nanoscale [34,35] [Fig. 1(a)]. It is also responsible for the structural integrity of sand castles in moist sand [36] [Fig. 1(b)], "craquelure" in paintings [Fig. 1(c)], and desiccation cracks in clayey soil [37,38] [Fig. 1(d)]—the latter two phenomena involving a combination of capillarity and shrinkage [39]. The powerful coupling among viscous, capillary, and frictional forces can give rise to spectacular patterns, including labyrinths [40] [Fig. 1(e)], corals, and stick-slip bubbles [41]. While the characteristic length scale of these morphologies is typically in the sub-centimeter range, they can determine the mode of gas release in nature at the kilometer scale, as is the case for methane venting from the seafloor [21] [Fig. 1(f)] and volatile gases from volcanic eruptions [42]—thus controlling critical flux exchanges in the Earth's global biogeochemical cycles.

This perspective is aimed at providing a brief overview of the state of knowledge, recent progress, and open questions at the confluence of multiphase hydrodynamics and mechanics of granular systems, with an emphasis on pattern formation. We first address the hydrodynamic components

*juanes@mit.edu

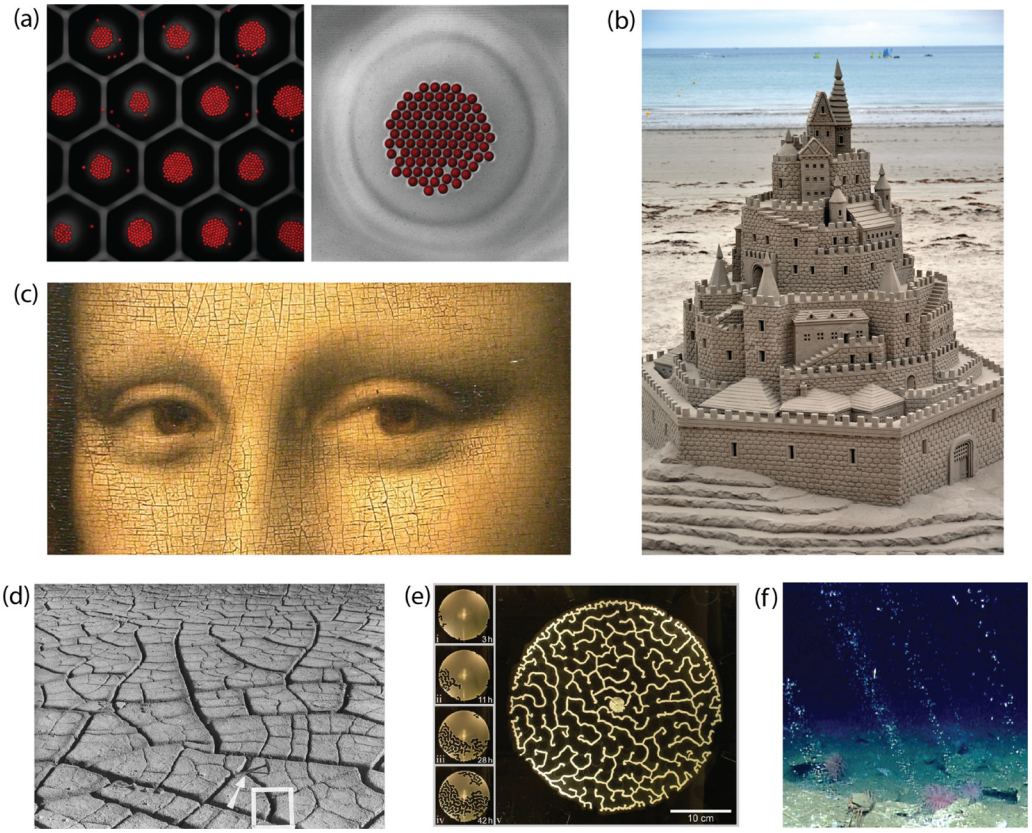

FIG. 1. Visual examples of the powerful interplay between multiphase fluids and the mechanics of granular media. (a) Particle self-assembly at the nanoscale (from Wang *et al.* [35]). (b) Sand castle in moist sand [192]. (c) Detail of craquelure [art credit: Mona Lisa (La Gioconda) by Leonardo da Vinci]. (d) Desiccation cracks on the soil surface (from Weinberger [43]). (e) Labyrinth patterns formed as a result of air invasion into a frictional suspension (from Sandnes *et al.* [40]). (f) Venting of methane bubbles from the ocean seafloor (from Skarke *et al.* [21]).

of the problem and describe fluid-fluid displacement in rigid porous media. We then extend the description to movable, deformable, and breakable granular media, thus accounting for the coupling between fluid and solid mechanics at the grain scale. We then focus on one particular aspect of this coupling: the role of wettability (the relative affinity of the solid grains to the different fluids in the pore space) on the morphology of granular-pack deformation from fluid injection. Finally, we point to fundamental knowledge gaps and exciting avenues of research.

II. MULTIPHASE FLOW IN RIGID POROUS MEDIA

We start by pointing to the fundamentally distinct nature of miscible (single-phase) and immiscible (multiphase) flow in rigid porous media, which is best done through an example [44]. Consider a porous medium such as a pack of glass beads filled with two density-mismatched fluids that share a vertical interface (Fig. 2). The different density of the fluids drives the lock-exchange flow, where the lighter fluid spreads along the top of the cell. If the two fluids are miscible, this flow is accompanied by a smooth deformation of the fluid-fluid front, from vertical towards horizontal [Fig. 2(a)]. In contrast, when the two fluids are immiscible, a segment of the interface remains indefinitely pinned in its original vertical configuration [Fig. 2(b)]. In order to fully appreciate the

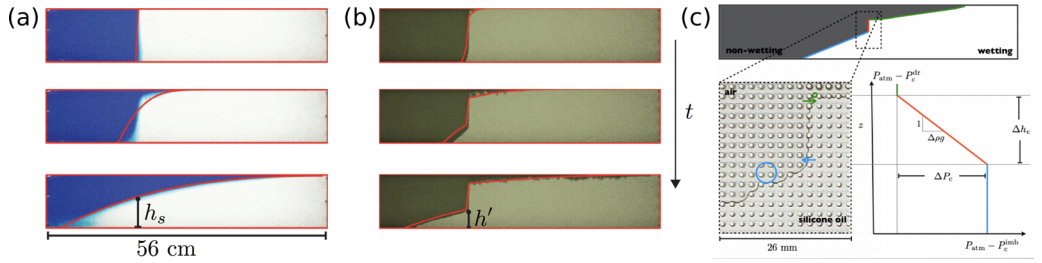

FIG. 2. Lock-exchange flow of (a) a miscible and (b) an immiscible fluid pair in a glass-bead pack. (c) Fluid-fluid interface pinning in a microfluidic chip. The interface de-pins and moves away from the vertical position only where the local pressure difference between the two fluids is greater than the threshold capillary entry pressure. Adapted from Zhao *et al.* [44].

mechanisms responsible for the striking difference between miscible and immiscible lock-exchange flow in Fig. 2, we need to define a few concepts.

When two fluids are immiscible, the boundary between them is sharp, and interfacial tension γ pulls along it. This tension is the result of dissimilarity in the molecular interactions of the two phases [45], which introduces the energy cost per unit area of the interface. As a result, the system tries to minimize the area of the fluid-fluid interface. In fact, in the absence of solid surfaces and body forces, the fluid with the smaller volume would roll up into a sphere. In the presence of a solid phase, the fluid-fluid interface intersects the solid surface at an angle θ, which we measure within the invading fluid. The contact angle θ is a measure of wettability—it reflects the affinity of the solid to the invading fluid phase. The system is in drainage when $\theta > 90^\circ$, and it is in imbibition when $\theta < 90^\circ$. Furthermore, there is a pressure drop (the Laplace pressure Δp [45]) associated with all fluid-fluid interfaces confined within the pore space. This pressure drop at each interface scales as

$$\Delta p \sim \frac{\gamma \cos\theta}{R}, \tag{1}$$

where R is the characteristic size of pore throats. Equation (1) anticipates the highest Laplace pressure drop across the invading front when it is in strong drainage ($\theta \to 180^\circ$) and when it passes through a narrow throat. The interface can get pinned locally if the invading fluid pressure is insufficient to overcome this local threshold capillary pressure.

In fact, the local threshold capillary pressures are responsible for the contrasting behavior of miscible and immiscible experiments in Fig. 2: the hydrostatic pressure difference across most of the vertical immiscible interface in Figs. 2(b) and 2(c) is insufficient to overcome the threshold capillary pressures and squeeze the immiscible interface across local constrictions in either direction. This is responsible for the permanent pinning of the fluid-fluid interface section in its initial vertical position. The fluid-fluid displacement depicted in Fig. 2 is an example of how pore-scale displacement mechanisms can shape the displacement patterns on a macroscopic scale—a hallmark of multiphase flow in porous media.

Much of our knowledge of fluid-fluid displacement in porous media has been acquired by examining displacement mechanisms at the pore scale [46]. The interplay between pore geometry and the positions of the local interfaces produces distinct pore-scale displacement scenarios, many of which are accompanied by rapid pressure changes [46]. Haines jumps are a prominent example of such pore-scale displacement mechanisms, where the invading fluid experiences a rapid change in curvature (and thus pressure) as it pushes through narrow pore constrictions [47–51]. This mechanism is prevalent in slow drainage, where sudden bursts of the local fluid-fluid interfaces are responsible for sharp fluctuations in the injection pressure signal [52,53]. In some cases, the speed of the Haines jumps was recorded to be 50 times larger than the mean front velocity [49] and was observed to cascade through tens of pores in a single jump event. Slow fluid-fluid

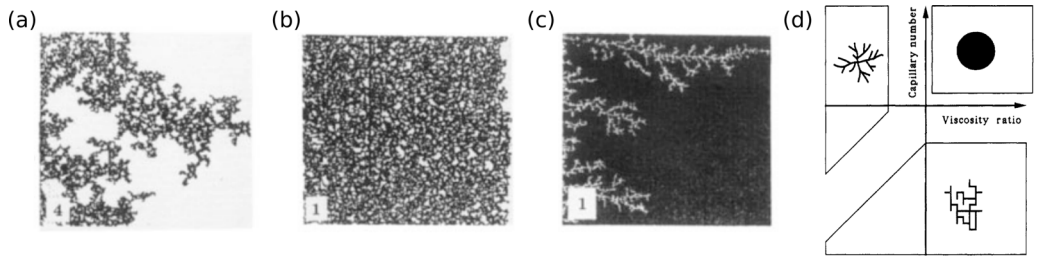

FIG. 3. Lenormand *et al.* [57] studied drainage in porous media and found that the fluid-fluid front can advance through (a) invasion percolation, (b) stable displacement, or (c) viscous fingering, depending on Ca and M. The character of displacement is synthesized in the (d) phase diagram of Lenormand *et al.* [57]. Adapted from Lenormand [58].

displacement in drainage produces distinct and robust patterns that are faithfully reproduced with invasion-percolation models [54,55], where the displacement front advances by invading pores with the lowest threshold capillary pressures first. This mode of displacement traps clusters of the defending fluid in two-dimensional porous media, producing a self-similar morphology of the invading fluid [56] [Fig. 3(a)].

The morphology of the displacement front changes significantly at high injection rates. When a more viscous fluid displaces a less viscous fluid, it does so through a compact front, removing most of the defending fluid from the pore space [Fig. 3(b)]. When a less viscous fluid displaces a more viscous fluid, the invasion front becomes unstable to small perturbations and advances through preferential flow paths [i.e., viscous fingering in Fig. 3(c)]. These viscous fingering patterns are also self-similar and bear a strong resemblance to diffusion-limited aggregation patterns [59–61].

Our classical understanding of fluid-fluid displacement in drainage has been synthesized in the seminal diagram of Lenormand *et al.* [57] [Fig. 3(d)]. Here, the character of the displacement is determined by two dimensionless parameters: the viscosity ratio of the two fluids $M \equiv \mu_i/\mu_d$, and the ratio of viscous to capillary forces $\mathrm{Ca} \equiv \mu_i u/\gamma$ (capillary number), where u is the characteristic speed of the displacement front, and μ_i and μ_d are the invading and defending fluid viscosities, respectively. One can tune the character of fluid-fluid displacement between viscous fingering, stable displacement, and invasion-percolation by changing Ca and M. Much of the Ca-M parameter space has been explored with both experiments [52,60,62] and pore-network models [54,55,57,61,63–73], and although Lenormand's phase diagram has been enormously influential and successful in organizing the current state of knowledge of fluid-fluid displacement in porous media, its applicability is restricted to systems in strong drainage.

There have been sustained efforts towards enhancing our knowledge of fluid-fluid displacement to account for wettability effects. A large number of core-scale experiments have shown improved displacement efficiency when the system's wettability is altered towards imbibition [74–78]. This was complemented by systematic studies of imbibition under favorable viscosity contrast ($M > 1$) [79–82] and quasistatic pore-network models that accounted for wettability effects [72,83–88]. More recent efforts have been summarized in Singh *et al.* [89] and include comprehensive studies of wettability effects during fluid-fluid displacement in glass bead packs [90] and microfluidic cells [91], as well as dynamic pore-network models that account for wettability effects [73,92]. Here, we build our discussion around the work of Zhao *et al.* [91] and subsequent numerical efforts of Primkulov *et al.* [72,73].

Zhao *et al.* [91] conducted a series of fluid-fluid displacement experiments in a quasi-two-dimensional porous medium, fabricated with soft lithography techniques by confining a circular post pattern between the two plates of a Hele-Shaw cell. All surfaces of the microfluidic chip were manufactured with a photocurable resin (NOA 81), where the degree of UV-light exposure is correlated with the surface wettability [93]. Zhao *et al.* [91] filled these wettability-controlled

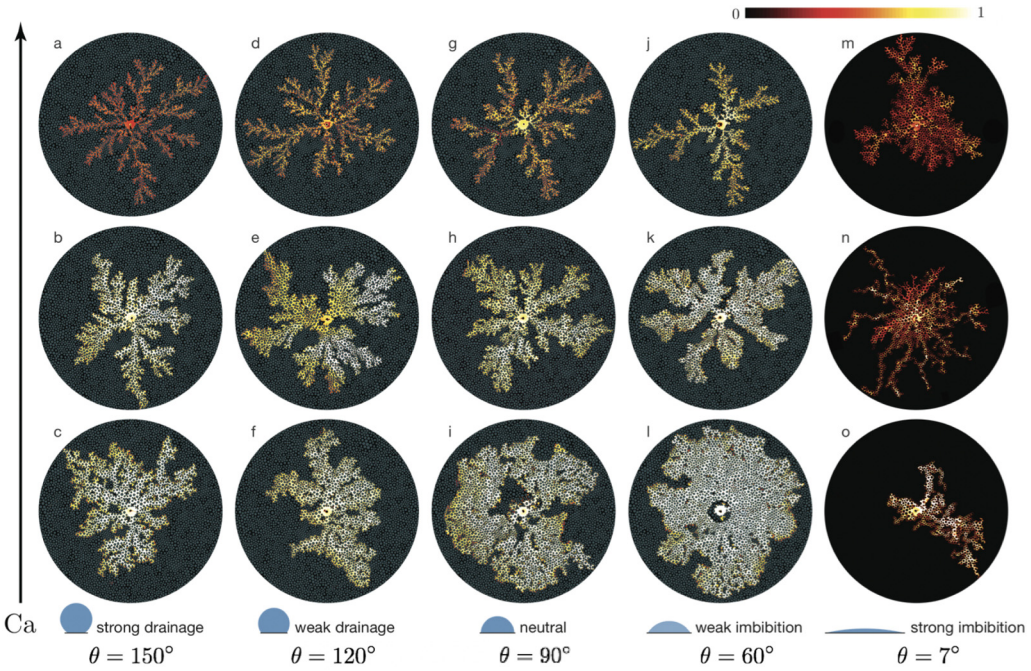

FIG. 4. Water displacing viscous silicone oil in wettability-controlled quasi-two-dimensional porous medium. Water was injected with different Ca under wettability ranging from strong drainage to strong imbibition. The displacement front was shown to advance through invasion percolation, cooperative filling, and corner flow at low Ca. At high Ca water advanced through viscous fingers, either leaving a film of oil or moving through films of water on the solid surfaces. Reprinted from Zhao *et al.* [91].

flow cells with viscous silicone oil and injected water from the center at controlled flow rates. The invading fluid patterns in such experiments (Fig. 4) change depending on Ca and θ, and it is best to describe them alongside the pore-scale mechanisms responsible for the change in patterns.

We first traverse the bottom row of experiments in Fig. 4, corresponding to the lowest injection rate and where viscous effects can be neglected. In this limit, the fluid invasion patterns are mainly governed by capillary forces. Cieplak and Robbins [83,84] defined three pore-scale events that are responsible for advancing the invading fluid front: "burst," "touch," and "overlap" (Fig. 5). The burst event corresponds to a stable interface that intersects the posts at prescribed θ and has a maximum possible curvature. Increasing the curvature (and therefore the Laplace pressure) above the burst configuration will render the interface unstable and the invading fluid will occupy the pore space ahead. The touch event corresponds to the interface contacting a nearby post and subsequently occupying the remainder of the pore. The overlap event takes place when two neighboring menisci overlap on or near a shared post. The burst events are prevalent in strong drainage ($\theta = 150^\circ$ in Fig. 4), while touch and overlap are prevalent near weak imbibition ($\theta = 60^\circ$ in Fig. 4): the relative frequency of these pore-scale events is responsible for the transition in patterns for $60^\circ < \theta < 150^\circ$. In strong drainage, the fluid-fluid displacement is incomplete, and clusters of the defending fluid are trapped behind the fluid front [Fig. 4(c)]. In weak imbibition, invading fluid patterns are compact [Fig. 4(l)]. As the wettability of the solid approaches strong imbibition ($\theta = 7^\circ$ in Fig. 4), the invading fluid no longer advances by occupying the pores completely. Instead, it advances by coating the corners at the intersection of posts with top and bottom plates (see "corner flow" in Fig. 5), which results in patterns equivalent to the one in Fig. 4(o) [72]. The entire bottom row of Fig. 4 can be

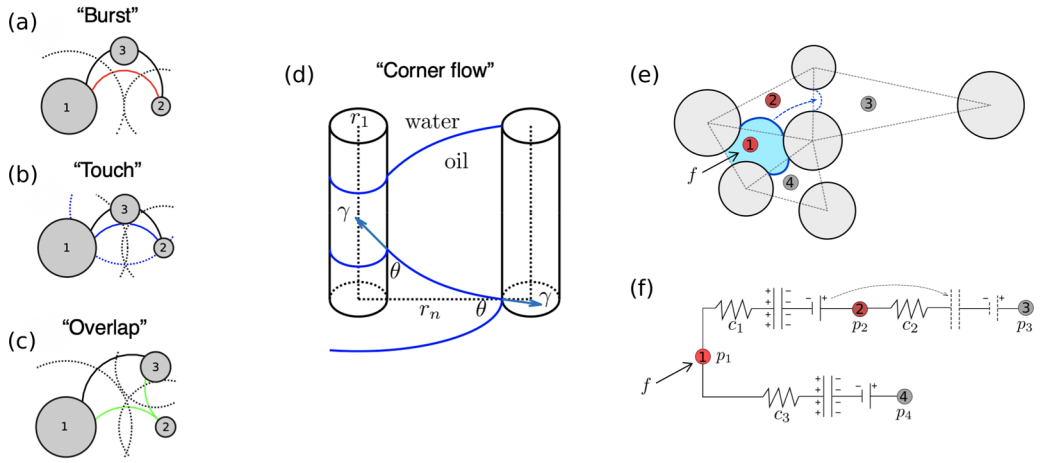

FIG. 5. Pore-scale displacement events that govern quasistatic fluid-fluid flow are (a) burst (i.e., Haines jump), (b) touch, (c) overlap (i.e., coalescence), and (d) corner flow (i.e., coating of posts with wetting fluid). These pore-scale events naturally augment the dynamic pore-network model ("moving-capacitor" model). The moving-capacitor model utilizes the analogy between (e) immiscible fluid-fluid displacement in porous media and (f) electrical current, where local fluid-fluid interfaces are represented through capacitors and event capillary entry pressures inform the voltage drop corresponding to dielectric breakdown in a capacitor. Adapted from Primkulov *et al.* [72] and Primkulov *et al.* [94].

modeled as an invasion-percolation model that accounts for arbitrary wettability of the solid surface by incorporating the four pore-scale events in the quasistatic limit [72].

The experiments corresponding to higher values of Ca in Fig. 4 can be modeled by adding viscous forces to the quasistatic model [72,73]. Here, it is convenient to draw an analogy between flow in porous media and currents in an electrical circuit: Poiseuille flow is equivalent to Ohm's law, conservation of mass is equivalent to Kirchhoff's rule, pore channels are represented with resistors, and local menisci are represented with capacitors [73]. In electrical circuits, capacitors experience dielectric breakdown when charges on their plates exceed a threshold value. Analogously, local menisci become unstable and enter a pore whenever the pressure difference across the interface exceeds critical Laplace pressure that corresponds to burst, touch, or overlap. This reduces the two-phase flow problem to a sequence of linear equations, and their solution allows recovering a phase diagram (Fig. 6) that captures the one obtained from experiments (Fig. 4). While our network modeling approach accurately captures the morphology of the invading fluid and its pressure signal over a wide range of Ca-M-θ space, it comes with a number of simplifying assumptions (e.g., simplified pore geometry, complete pistonlike displacement within individual pore throats in all regimes except corner flow) that make it computationally efficient. In fact, the model has been critically compared with other state-of-the-art pore-scale models [95].

III. MULTIPHASE FLOW IN DEFORMABLE GRANULAR MEDIA

When the porous medium is not rigid, there is an interplay between fluid flow and the mechanics of deformation of the medium. Such interplay is relevant across spatial scales, from the pore scale [96–100] to the geologic scale [21,42,101,102]. Here, we focus on giving a brief account of this interplay in granular media, with an emphasis on the grain-scale mechanisms that control pattern formation.

The motion of the granular pack can occur in the presence of single-phase flow. For example, groundwater flow can cause the erosion of surface sediments [103], leading to channelization of the flow and incision of river beds in the landscape [104]. Similar physics are responsible for

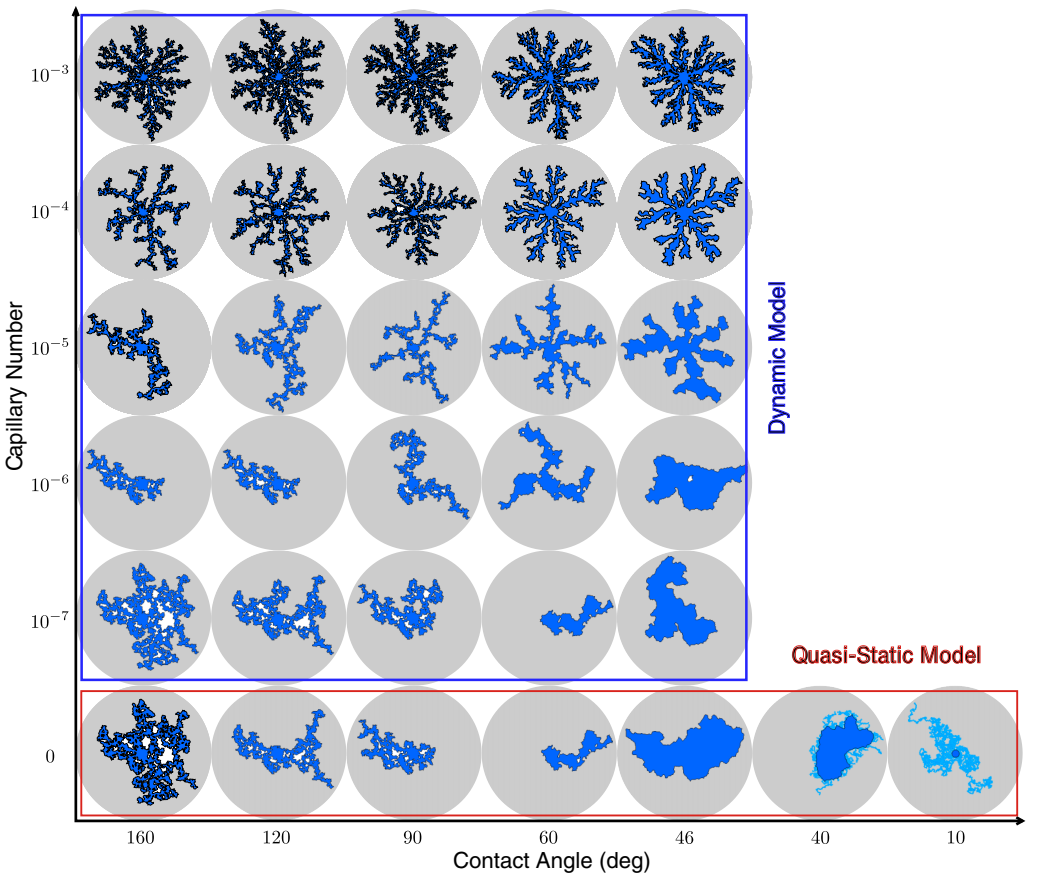

FIG. 6. Numerical simulation of fluid-fluid displacement under different Ca and wettability using quasistatic [72] and dynamic moving-capacitor [73] models. The simulations cover the majority of the Ca-M parameter space along with the dominant flow regimes demonstrated in experiments (Fig. 4). Adapted from Primkulov *et al.* [73].

sand mobilization and production from wells in poorly consolidated sedimentary rocks [105], whereby cohesion and friction in the granular material are overcome by the hydrodynamic forces that dislodge the contacts and mobilize the grains.

Another classic example of medium deformation under single-phase flow is hydraulic fracturing [106], which is typically understood as a result of overcoming the tensile strength of a poroelastic medium upon rapid fluid injection, such that the pore pressure builds faster than it dissipates through the medium [107]. In the context of fine-grained media like clay slurries and colloidal suspensions, Van Damme *et al.* [108] and Lemmaire *et al.* [109] first identified that a (viscoelastic) fracturing regime could be reached as a transition from the viscous fingering regime. This transition was strongly controlled by the Deborah number, De, where for $\mathrm{De} \ll 1$ viscous effects dominate, whereas for $\mathrm{De} \gg 1$ the system behaves as an elastic solid. A recent study on a system of a two-dimensional (2D) monolayer of elastic frictionless hydrogel particles showcased inelastic deformation, resulting in the formation of an injection cavity from the collective rearrangement of the particles [110].

Here we are interested in *multiphase* fluid systems, where two or more fluid phases coflow through the granular medium. The fundamental notion in extending the description of multiphase flow in rigid porous media is that one must account for the possibility that the grains may

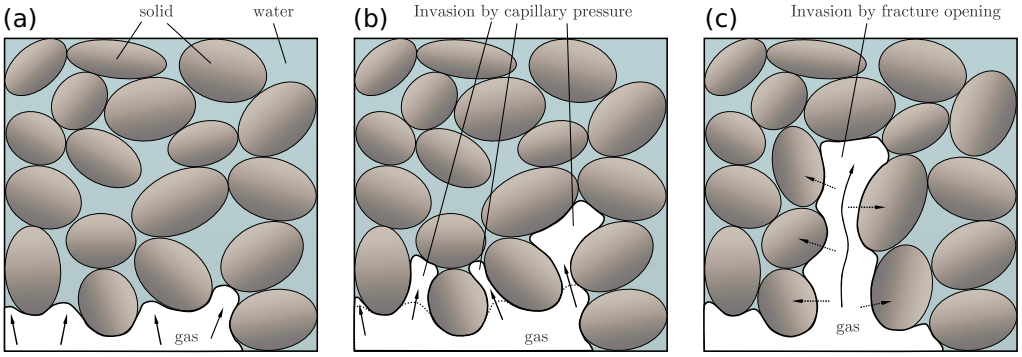

FIG. 7. Schematic diagram of the two modes of fluid–fluid displacement (gas-water) in a deformable granular medium. (a) The fluid-fluid interface before displacement. (b) Fluid invasion when the medium behaves rigidly. (c) Invasion by conduit opening; the exerted fluid pressure is sufficient to overcome confinement, cohesion and friction at grain contacts. Reprinted from Jain and Juanes [111].

move as a result of the fluid-fluid displacement (Fig. 7). This picture at the grain scale makes it apparent that surface-tension forces need to be invoked in the description of the system's evolution [38,40,96,100,111–113].

A. Gas venting

An area that has received substantial attention is the migration of gas within (and subsequent release out of) soft, organic-rich, aquatic sediments [19–21]. From a geoscience perspective, this problem is central to understanding methane fluxes and the global carbon cycle, including its dependence on, and feedback to, climate change [22]. There is by now indisputable direct evidence of widespread methane venting from the seafloor [19,21,114–118], shallow and deep lake sediments [20,119–123], and man-made reservoirs [124]. This concept of conduit opening in unconsolidated sediments has also been invoked to explain gas migration at geologic spatial and time scales [101,102,125,126].

To explain these phenomena, several groups have conducted controlled laboratory experiments of vertical gas migration in unconsolidated granular materials, almost exclusively in 2D or quasi-2D systems (a Hele-Shaw cell packed with beads or grains). These studies have led to direct observations of the morphology of air invasion, delineating conditions under which the granular pack behaves rigidly or opens conduits for gas migration [127–130]. In particular, the mode of invasion can transition from fingering to fracturing during the course of a single experiment, as the gas (injected at the bottom of the cell) migrates upwards to regions of the granular pack subject to lower confining stress [131]. In soft systems, the interplay between elasticity, confinement, and buoyancy can lead to a range of mixed gas-migration regimes and the emergence of episodic capture-venting dynamics [132].

Some 3D experimental systems have investigated the surface footprint of venting dynamics, either from point gas injection in granular media [133] or from actual *in situ* methane generation in lake-mud incubation experiments [134]. Only recently have experimental studies addressed the 3D dynamics of vertical gas migration in deformable granular media through direct visualization. Sun and Santamarina [135] employed fumed silica and a refractive-index-matching oil blend and two orthogonal camera views for partial 3D characterization of the gas migration process. Dalbe and Juanes [136] developed an experimental setup to fully reconstruct the coupled invasion-deformation dynamics in 3D. They constructed a porous cell made of borosilicate glass beads, filled it with glycerol to achieve refractive-index matching, and injected less-viscous silicon oil that is also index-matched. They employed a planar laser-induced fluorescence (PLIF) technique in which a laser

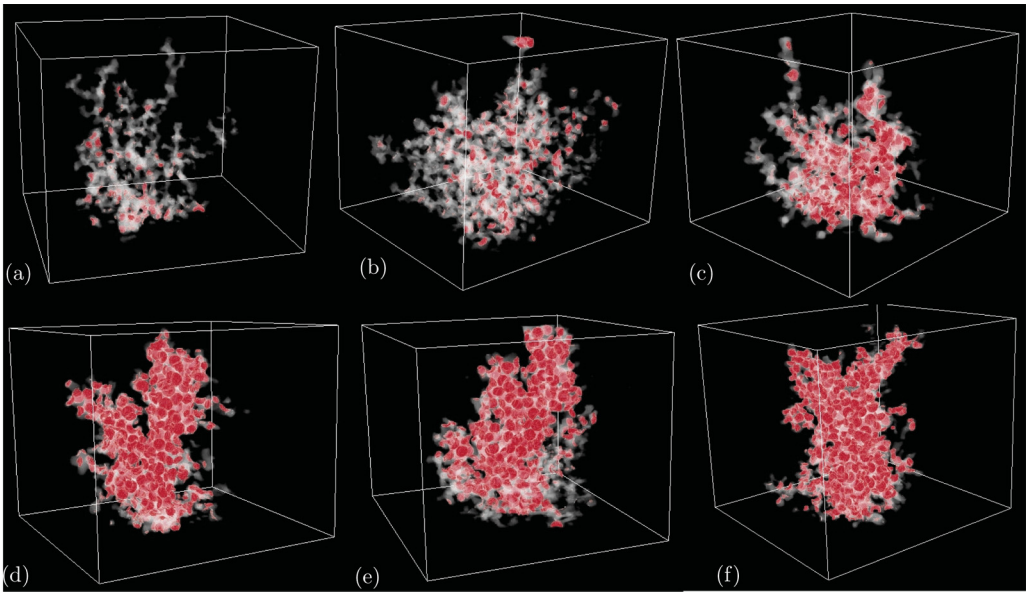

FIG. 8. 3D PLIF reconstructions of the fluid invasion pattern (in white) superimposed on the conduit opening (in red) for experiments in which a fluid (silicon oil) is injected at the bottom of a pack of glass beads to displace a more viscous fluid (glycerol). Reprinted from Dalbe and Juanes [136].

sheet, mounted on a moving stage, shines on the medium and excites fluorescent dyes premixed with the defending and invading fluids. This technique allowed them to reconstruct the 3D dynamics of the granular pack at the subpore scale (Fig. 8).

B. Desiccation cracks

The phenomenon of desiccation cracks is a common occurrence in drying soil [43,137] and paint [138,139], often leading to polygonal patterns [140] [Figs. 1(c) and 1(d)]. Controlled laboratory experiments on monolayer packings [97,98], colloidal suspensions [141–143], and soil systems [37,137,144] have paved the way for improved understanding and modeling at the particle level [38,97,98,145–148] and, recently, at the continuum level using phase-field models [149,150].

This cumulative understanding has elucidated the critical role of capillary forces in the initiation and propagation of cracks [38] and the dominant control of shrinkage in determining the characteristic size of the cracked patterns—something that has recently been demonstrated with an analog hydrogel model, where the individual particles undergo shrinkage and swelling [39,151].

C. Frictional flows

The morphology of fluid invasion and granular deformation is ultimately determined by the interplay among viscous forces, capillary forces, and interparticle forces. Interparticle forces can have different origins, including cementation and cohesion at particle contacts that lead to tensile strength, and friction between particles, which depends strongly on the grain material, particle roughness, and degree of confinement—itself a function of packing fraction and confining stress.

This interplay was studied in depth in a series of investigations of so-called “frictional flows” [40,41]. In this experimental setup, air is injected to displace a layer of beads submerged in a defending fluid within a Hele-Shaw cell [Fig. 9(a)]. As the layer of beads is displaced, beads accumulate at the air-fluid interface, forming a front of dense bead-pack ahead of the interface [Fig. 9(b)]. The air injection rate controls the balance between viscous and capillary forces, and the

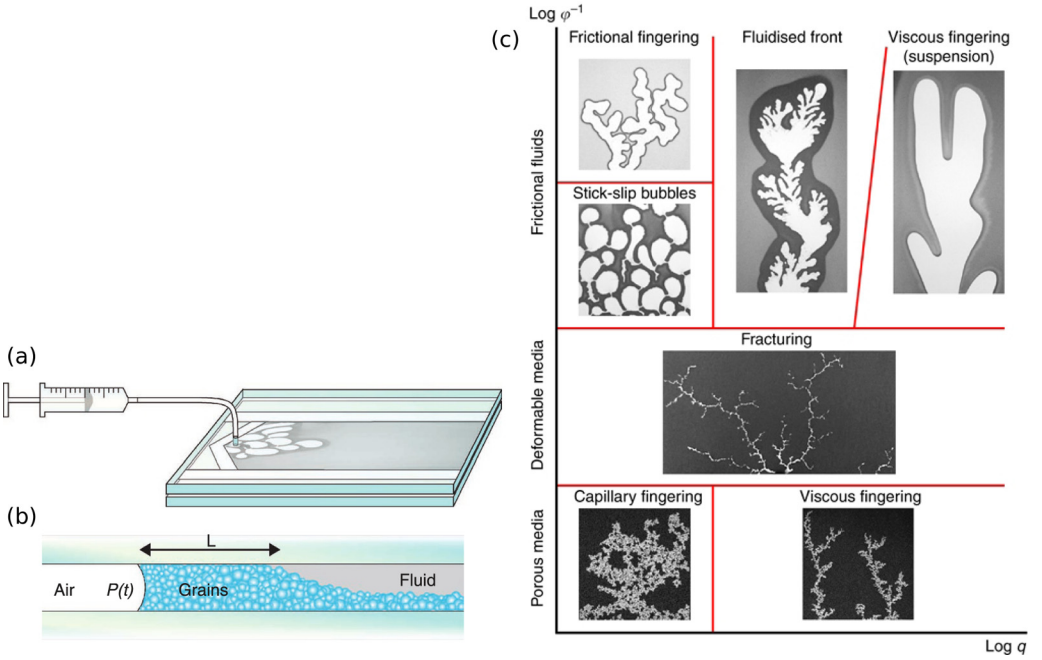

FIG. 9. Schematic of the experimental setup for frictional flows: (a) air is injected into a Hele-Shaw cell loaded with polydisperse glass beads that have settled in a water-glycerol solution; (b) the invading air-fluid interface accumulates a front of close-packed grains in the gap between the plates. (c) Phase diagram of frictional-flow morphologies in the space of the injection rate (increasing to the right) and the packing density (decreasing to the top). Reprinted from Sandnes *et al.* [41].

initial packing fraction of the suspension controls the degree of confinement. At a given packing fraction, low injection rates result in frictional invasion, characterized by frictional fingers or stick-slip bubbles. For the same packing fraction, as the injection rate increases, there is a transition in invasion morphology to one dominated by a fluidized front and coral-like patterns and, ultimately, to the classic Saffman-Taylor finger in viscous fluids [152] [Fig. 9(c)]. The invasion patterns and dynamics are also affected by the compressibility of the system [41,153] and the presence of a gravitational potential [154].

Of particular interest is what happens as the packing fraction increases, that is, as the system moves from a loose segregated suspension to a dense granular pack. The invasion pattern then undergoes another transition, from frictional flow to fracturing and from fracturing to fluid-fluid displacement in a rigid medium [Fig. 9(c)]. To quantitatively understand this morphological transition, Holtzman *et al.* [112] conducted experiments of air invasion into a Hele-Shaw cell with a liquid-saturated granular pack, in which the degree of confinement was controlled not by the packing fraction but, rather, by the confining stress [Fig. 10(a)]. At sufficiently high confining stress, the granular pack behaves as a rigid porous medium. The morphology of air invasion is then determined by the capillary number Ca, and exhibits a transition from capillary fingering to viscous fingering. This transition occurs when the characteristic macroscopic viscous pressure drop in the direction parallel to flow, δp_{v}, is balanced with the variation in capillary entry pressures along the interface, δp_{c}. The condition $\delta p_{\mathrm{v}} \sim \delta p_{\mathrm{c}}$ is controlled by a "modified capillary number" [112,155,156]:

$$\mathrm{Ca}^{*} = \underbrace{\frac{\eta(Q/bd)}{\gamma}}_{\mathrm{Ca}} \frac{R}{d}, \tag{2}$$

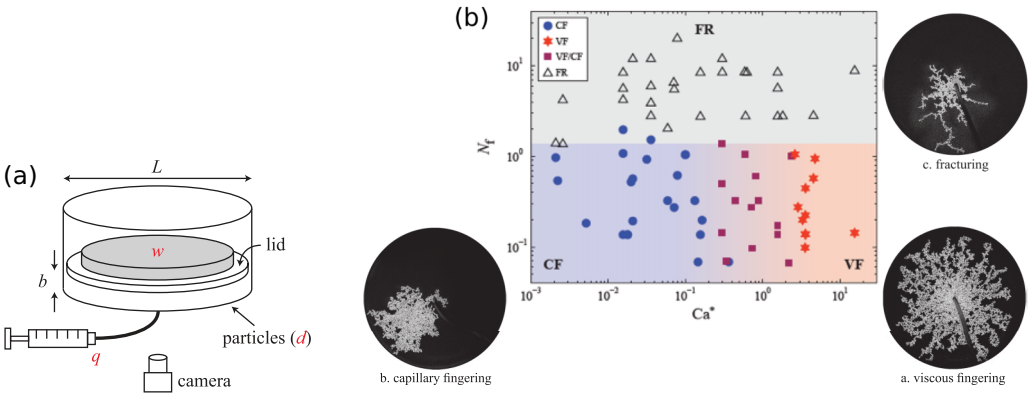

FIG. 10. (a) Experimental setup of hydrocapillary fracturing experiments, where a thin bed of water-saturated glass beads is confined in a cylindrical acrylic cell, subject to a weight placed on a disk that rests on top of the beads. Air is injected into the center of the cell at a fixed flow rate. (b) Phase diagram of drainage in granular media, showing three invasion regimes: viscous fingering (VF), capillary fingering (CF), and fracturing (FR). The tendency to fracture is characterized by the fracturing number N_f: drainage is dominated by fracturing in systems with $N_f \gg 1$. At lower N_f values, the type of fingering depends on the modified capillary number, Ca^*. Adapted from Holtzman *et al.* [112].

where Ca is the classic capillary number [57], Q is the injection rate, b is the height of the cell, d is the grain size, and R is the cell radius.

As the confining stress decreases, the granular pack loses its rigidity and is subject to grain motion concomitant with fluid invasion. In a granular medium, conduits open when forces exerted by the fluids exceed the mechanical forces that resist particle rearrangements. In cohesionless granular material, these forces include elastic compression and friction. For systems with densely packed, highly compliant frictionless particles, conduit opening is controlled by particle deformation [132]. However, for many types of particles including most mineral grains and manufactured beads, the high particle stiffness limits interparticle compression, making frictional sliding the dominant deformation mechanism that alters the pore geometry [112,157].

The emergence of fracturing is determined by the so-called "fracturing number," N_f, that measures the system deformability as the ratio of the pressure forces that drive fracturing (capillary pressure, γ/d, and local viscous pressure drop, $\nabla p_v d \sim \eta v/d$) and the resisting force due to friction [112]:

$$N_f = \frac{(\gamma/d)(1+\mathrm{Ca})}{\mu\sigma'}, \tag{3}$$

where μ is the coefficient of friction, and $\sigma' \sim W/R^2$ is the effective confining stress, with W being the weight on top of the cell.

Indeed, the two transitions are observed experimentally: from capillary fingering to viscous fingering at $Ca^* \sim 1$ at high confining stresses, and from either capillary fingering or viscous fingering to fracturing at $N_f \sim 1$ (Fig. 10). While the transition to fracturing from viscous pressure drop is relatively well understood and is the basis for hydraulic fracturing [106,107], the work of Holtzman *et al.* [112] demonstrates that the transition to a granular fracturing regime can occur as *capillary fracturing*, at vanishing flow rates.

IV. IMPACT OF WETTABILITY ON FRICTIONAL FLOWS

Given the wealth of evidence demonstrating the importance of capillarity on deformation and fracture of granular media [41,112,157–159], the fundamental question that arises and has remained

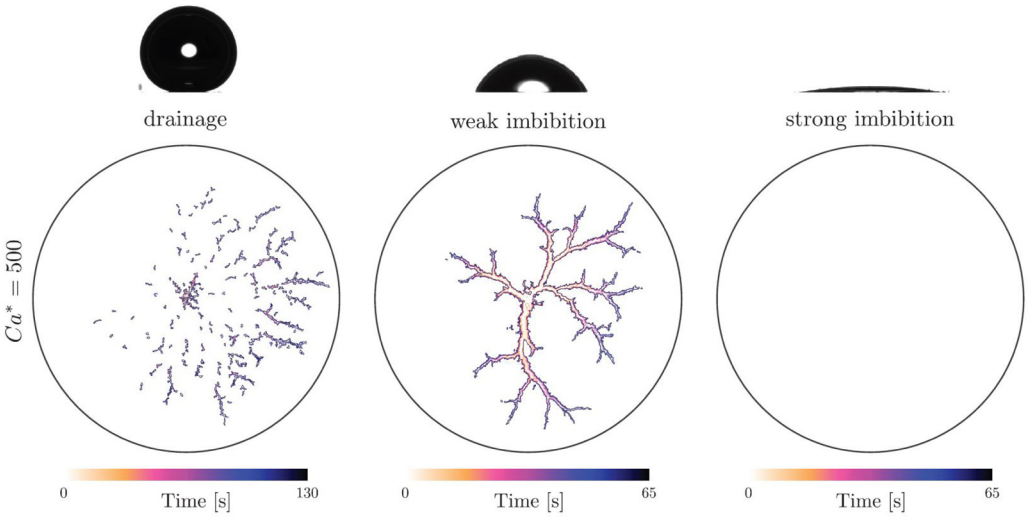

FIG. 11. Comparison of fracture networks that develop for different wettability conditions (strong drainage, weak imbibition, and strong imbibition), under the same modified capillary number and confining stress. Shown are the contours of the evolving fracture patterns at different times during injection (see color map). Adapted from Trojer *et al.* [160].

unexplored until very recently is how wetting properties impact the emergence of granular fracture and the ensuing fracture pattern.

To investigate the impact of wetting on fracturing of granular media, Trojer *et al.* [160] used an experimental setup similar to that of Holtzman *et al.* [112]—in which a low-viscosity fluid is injected into a circular Hele-Shaw cell filled with a dense glass-bead pack that is saturated with a more viscous, immiscible fluid—but now carefully tailoring the wettability of the fluid pair to the glass. The key result is a comparison of the fluid invasion patterns that develop for different wettability conditions (Fig. 11). The results demonstrate that the fracture morphology exhibits a nonmonotonic dependence on wettability: highly ramified, disconnected, and ephemeral fracturing in drainage (Fig. 11, left); robust, hierarchical, and persistent fracturing in weak imbibition (Fig. 11, center); and no fracturing in strong imbibition (Fig. 11, right). The physical mechanism responsible for the striking differences in the fracture morphology is a transition in the pore-scale fluid displacement from pore invasion in drainage to cooperative filling in weak imbibition to corner flow in strong imbibition.

These experimental observations indicate that wettability plays a fundamental role in fracturing of granular media, even at high capillary numbers when viscous forces dominate. In an effort to understand this behavior, Meng *et al.* [161] developed a fully coupled dynamic model of multiphase flow and granular mechanics at the grain scale. The fluid-fluid displacement is simulated by the moving capacitor dynamic network model described earlier [73], which explicitly incorporates the impact of wettability. The dynamic flow network model is coupled with a discrete element model [162], which simulates the mechanics of the granular pack by solving the linear and angular momentum balance equations of the many-body system with appropriate frictional-elastic interaction laws at the interparticle contacts [163]. To capture the two-way hydromechanical coupling, the pore-pressure forces are applied to the particles, leading to deformation and rearrangement, and particle motions feed back into pressure calculations by changing the pore-network geometry and topology.

Meng *et al.* [161] simulated the injection of a less viscous fluid into a frictional granular pack initially saturated with a more viscous, immiscible fluid, at an injection rate slow enough that

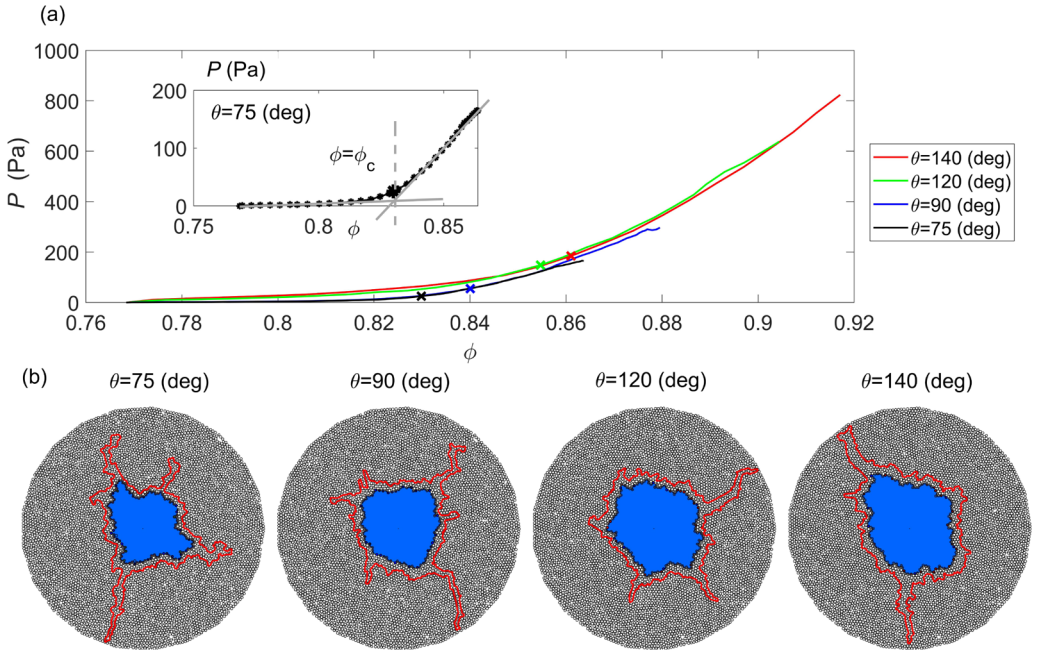

FIG. 12. Jamming transition analysis for the same injection rate and initial packing fraction ($\phi_0 = 0.77$) and four different wetting conditions ranging from weak imbibition to drainage: $\theta = 75^\circ$, 90°, 120°, and 140°. (a) Mean particle stress P as a function of packing density ϕ in the compacting granular layer. Inset: Determination of the critical packing fraction at jamming, ϕ_c, for $\theta = 75^\circ$. (b) Interface morphology at the jamming transition identified from panel (a) (black line), compared with that at breakthrough—when the invading fluid first reaches the outer boundary (red line). The comparison confirms that the jamming transition determines the onset of fracturing and that this transition occurs earlier in imbibition ($\theta = 75^\circ$) than in drainage ($\theta = 140^\circ$). Adapted from Meng *et al.* [161].

viscous pressure gradients were dissipated between front movements and capillary effects governed the displacement [53]. The simulations show that fluid invasion first occurs by the expansion of a cavity, followed by fracturing [Fig. 12(b)].

Remarkably, they also show that a decrease in θ—that is, transitioning from drainage to weak imbibition—leads to an earlier onset of fracturing, as evidenced by the smaller size of the fluid cavity [Fig. 12(b)]. This behavior cannot be explained by the evolving injection pressure level, the evolving packing fraction outside the cavity, or the volume of fluid injected alone. Indeed, the transition to fracturing for different wetting conditions occurs at different injection pressures, packing fractions, and injected volumes [161].

To rationalize this behavior, Meng *et al.* [161] hypothesized that the emergence of fracturing is akin to a phase transition from liquidlike to solidlike behavior and, thus, that it can be understood as a *jamming transition*. The classic metrics that characterize the jamming transition in dry granular media [164,165], such as the mean particle stress P rising from a near-zero background as a function of the evolving mean packing fraction ϕ, can be used to determine the critical packing fraction ϕ_c at which the jamming transition occurs [Fig. 12(a), inset]. This transition point from the jamming analysis agrees with the simulation results, which show that granular-pack deformation after jamming occurs almost exclusively by fracturing [Fig. 12(b)].

The coupled multiphase flow–mechanics grain-scale model was used to explore the rich emerging behavior as a function of two parameters, the contact angle θ varying from 140° (drainage) to 46° (imbibition), and the initial packing density ϕ_0 varying from 0.68 (loose pack) to 0.84 (dense

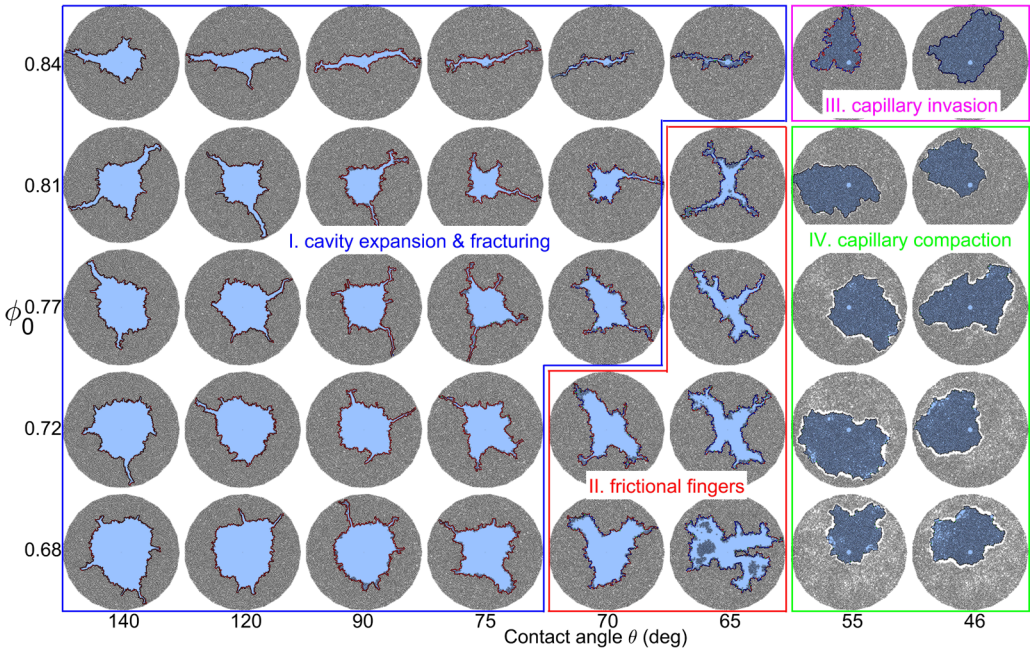

FIG. 13. Visual phase diagram of the invading fluid morphology at breakthrough corresponding to different substrate wettabilities (contact angle θ) and initial packing densities ϕ_0. Four distinct morphological regimes are identified: (I) cavity expansion and fracturing, (II) frictional fingers, (III) capillary invasion, and (IV) capillary compaction. Reprinted from Meng *et al.* [161].

pack). Figure 13 depicts the distinct morphological regimes that arise from injection as a visual phase diagram for different values of θ and ϕ_0. The patterns are categorized into four different regimes: (I) cavity expansion and fracturing, (II) frictional fingers, (III) capillary invasion, and (IV) capillary compaction. The system's response, and the transitions among the different regimes, can be synthesized in the form of a phase diagram of jamming in wet granular media [161], which extends its classic counterpart for dry granular systems [166].

V. OUTLOOK

Although much progress has been achieved in accounting for wettability effects with dynamic pore-network models in rigid porous media, many challenges still remain. The state-of-the-art dynamic pore network models are limited to system wettabilities between strong drainage and weak imbibition [73,95]. With this knowledge, however, it should be possible to update Lenormand's Ca-M diagram for drainage [57] [Fig. 3(d)] and account for wettability with contact angle θ as a third axis [94]. From a modeling standpoint, the strong imbibition regime in porous media has, so far, only been explored with a quasistatic model [72], and it would be interesting to extend this to a dynamic description.

Existing dynamic pore-network models that are able to account for wettability [73,92] do so for the paradigmatic case of cylindrical obstacles confined between two plates of Hele-Shaw cells [83,84,91]. As the next step, one could extend these models to a monolayer configuration, similar to the one used in many experiments [39,52,53,60,110,167]. Eventually, the quasistatic models that account for wettability [72,83,84] should be extended to three-dimensional bead packs and augmented to incorporate dynamic effects [73]. These efforts would yield important insights into the grain-scale mechanisms at play [161] in actual 3D systems.

From an experimental standpoint, the strong imbibition regime has been studied only under a very limited set of conditions [91,168], and much of the Ca-M parameter space in this regime has yet to be systematically explored. In particular, it would be interesting to study the statistics of invasion avalanches in the coating of posts at low Ca and characterize the universality class of this fluid-fluid displacement regime. Another important question pertaining to fluid-fluid displacement in rigid porous media is the post-breakthrough behavior, that is, the evolution of fluid occupancy *after* the invading fluid has reached the outlet—a process of direct relevance to hydrocarbon recovery and nonaqueous phase liquid remediation, but which has only recently started to be investigated [e.g., Ref. 168].

A frontier in the experimental investigation of the interplay between fluid and solid mechanics of granular media is the ability to directly characterize the evolution of stresses. While following the deformation of the granular pack with particle tracking or digital image correlation [157,160] may allow *inferring* the stress field at the particle scale [169–171], no experimental system has so far permitted direct visualization of the interparticle forces in granular packs subject to fluid injection and pore-pressure variations. To experimentally visualize stresses in coupled granular-fluid systems, photoelasticity is a promising technique. Photoelasticity has been used as an experimental technique to quantify the internal stresses within solid bodies for decades [172], and it provides a wealth of microscopic observables in assemblies of cylindrical disks, including contact forces [173,174], length and orientation of force chains [175], particle coordination number [176], and stick-slip behavior [177], that are vital for gaining a deeper understanding of the macroscopic behavior of granular systems. It would be enormously useful to extend this technique to poromechanical granular systems that, contrary to assemblies of cylindrical disks, have a connected pore space through which fluid can flow and fluid-fluid interfaces can move.

Finally, the frictional response of pore-granular media plays a central role in geohazards like landslides [178,179] and earthquakes [180,181]. There is a need for continuing to advance our fundamental understanding of the frictional behavior of granular material [182] under fluid pressurization [183–188] and in the presence of multiphase fluids, and to develop improved constitutive models [189,190] that honor the microscale physics and capture the seismic-aseismic transitions in friction. This knowledge would elicit intriguing questions for the prediction of geohazards, including whether it is possible to find precursors—such as microtremors—to the onset of catastrophic failure in landslides [179] and, conversely, precursors—such as creep aseismic deformation—to the onset of seismic, runaway-slip failure in earthquakes [187,191].

ACKNOWLEDGMENTS

This work was supported by the U.S. Department of Energy (Grant No. DE-SC0018357) and the U.S. National Science Foundation (Grant No. CMMI-1933416).

[1] R. E. Horton, The role of infiltration in the hydrologic cycle, Trans., Am. Geophys. Union **14**, 446 (1933).

[2] J. R. Philip, Theory of infiltration, in *Advances in Hydroscience*, edited by V. T. Chow (Academic, New York, 1969), pp. 215–296.

[3] D. E Hill and J.-Y. Parlange, Wetting front instability in layered soils, Soil Sci. Soc. Am. J. **36**, 697 (1972).

[4] L. Cueto-Felgueroso and R. Juanes, Nonlocal Interface Dynamics and Pattern Formation in Gravity-Driven Unsaturated Flow through Porous Media, Phys. Rev. Lett. **101**, 244504 (2008).

[5] A. Porporato, P. D'Odorico, F. Laio, L. Ridolfi, and I. Rodriguez-Iturbe, Ecohydrology of water-controlled ecosystems, Adv. Water Resour. **25**, 1335 (2002).

[6] A. Porporato, E. Daly, and I. Rodriguez-Iturbe, Soil water balance and ecosystem response to climate change, Am. Nat. **164**, 625 (2004).

[7] D. deB. Richter and M. L. Mobley, Monitoring Earth's critical zone, Science **326**, 1067 (2009).
[8] T. H. Illangasekare, J. L. Ramsey, K. H. Jensen, and M. B. Butts, Experimental study of movement and distribution of dense organic contaminants in heterogeneous aquifers, J. Contam. Hydrol. **20**, 1 (1995).
[9] K. D. Pennell, G. A. Pope, and L. M. Abriola, Influence of viscous and buoyancy forces on the mobilization of residual tetrachloroethylene during surfactant flushing, Environ. Sci. Technol. **30**, 1328 (1996).
[10] S. Bachu, W. D. Gunther, and E. H. Perkins, Aquifer disposal of CO_2: Hydrodynamic and mineral trapping, Energy Convers. Manage. **35**, 269 (1994).
[11] K. S. Lackner, A guide to CO_2 sequestration, Science **300**, 1677 (2003).
[12] F. M. Orr, Jr., Storage of carbon dioxide in geologic formations, J. Pet. Technol. **56**, 90 (2004).
[13] IPCC, *Special Report on Carbon Dioxide Capture and Storage*, edited by B. Metz *et al.* (Cambridge University, Cambridge, England, 2005).
[14] S. Bachu, CO_2 storage in geological media: Role, means, status and barriers to deployment, Prog. Energy Combust. Sci. **34**, 254 (2008).
[15] M. L. Szulczewski, C. W. MacMinn, H. J. Herzog, and R. Juanes, Lifetime of carbon capture and storage as a climate-change mitigation technology, Proc. Natl. Acad. Sci. U.S.A. **109**, 5185 (2012).
[16] F. M. Orr, Jr. and J. J. Taber, Use of carbon dioxide in enhanced oil recovery, Science **224**, 563 (1984).
[17] L. W. Lake, *Enhanced Oil Recovery* (Prentice-Hall, Englewood Cliffs, NJ, 1989).
[18] L. Cueto-Felgueroso and R. Juanes, Forecasting long-term gas production from shale, Proc. Natl. Acad. Sci. U.S.A. **110**, 19660 (2013).
[19] N. Shakhova, I. Semiletov, A. Salyuk, V. Yusupov, D. Kosmach, and Ö. Gustafsson, Extensive methane venting to the atmosphere from sediments of the East Siberian Arctic shelf, Science **327**, 1246 (2010).
[20] D. Bastviken, L. J. Tranvik, J. A. Downing, P. M. Crill, and A. Enrich-Prast, Freshwater methane emissions offset the continental carbon sink, Science **331**, 50 (2011).
[21] A. Skarke, C. Ruppel, M. Kodis, D. Brothers, and E. Lobecker, Widespread methane leakage from the sea floor on the northern US Atlantic margin, Nat. Geosci. **7**, 657 (2014).
[22] C. Ruppel and J. D. Kessler, The interaction of climate change and methane hydrates, Rev. Geophys. **55**, 126 (2017).
[23] C. Y. Wang, Fundamental models for fuel cell engineering, Chem. Rev. **104**, 4727 (2004).
[24] C. H. Lee, B. Zhao, R. Abouatallah, R. Wang, and A. Bazylak, Compressible-Gas Invasion into Liquid-Saturated Porous Media: Application to Polymer-Electrolyte-Membrane Electrolyzers, Phys. Rev. Appl. **11**, 054029 (2019).
[25] H. A. Stone, A. D. Stroock, and A. Ajdari, Engineering flows in small devices: Microfluidics toward a laboratory-on-a-chip, Annu. Rev. Fluid Mech. **36**, 381 (2004).
[26] A. A. Darhuber and S. M. Troian, Principles of microfluidic actuation by modulation of surface stresses, Annu. Rev. Fluid Mech. **37**, 425 (2005).
[27] G. M. Whitesides, The origins and the future of microfluidics, Nature (London) **442**, 368 (2006).
[28] H.-W. Lu, K. Glasner, A. L. Bertozzi, and C.-J. Kim, A diffuse-interface model for electrowetting drops in a Hele-Shaw cell, J. Fluid Mech. **590**, 411 (2007).
[29] W. Song, T. W. de Haas, H. Fadaei, and D. Sinton, Chip-off-the-old-rock: The study of reservoir-relevant geological processes with real-rock micromodels, Lab Chip **14**, 4382 (2014).
[30] M. L. Porter, J. Jiménez-Martínez, R. Martinez, Q. McCulloch, J. W. Carey, and H. S. Viswanathan, Geo-material microfluidics at reservoir conditions for subsurface energy resource applications, Lab Chip **15**, 4044 (2015).
[31] W. Song and A. R. Kovscek, Functionalization of micromodels with kaolinite for investigation of low salinity oil-recovery processes, Lab Chip **15**, 3314 (2015).
[32] S. A. Kelly, C. Torres-Verdin, and M. T. Balhoff, Subsurface to substrate: Dual-scale micro/nanofluidic networks for investigating transport anomalies in tight porous media, Lab Chip **16**, 2829 (2016).
[33] S. M. Prakadan, A. K. Shalek, and D. A. Weitz, Scaling by shrinking: Empowering single-cell 'omics' with microfluidic devices, Nat. Rev. Genet. **18**, 345 (2017).
[34] N. Chakrapani, B. Wei, A. Carrillo, P. M. Ajayan, and R. S. Kane, Capillarity-driven assembly of two-dimensional cellular carbon nanotube foams, Proc. Natl. Acad. Sci. U.S.A. **101**, 4009 (2004).

[35] W. Wang, J. V. I. Timonen, A. Carlson, D.-M. Drotlef, C. T. Zhang, S. Kolle, A. Grinthal, T.-S. Wong, B. Hatton, S. H. Kang, S. Kennedy, J. Chi, R. T. Blough, M. Sitti, L. Mahadevan, and J. Aizenberg, Multifunctional ferrofluid-infused surfaces with reconfigurable multiscale topography, Nature (London) **559**, 77 (2018).
[36] D. J. Hornbaker, R. Albert, I. Albert, A.-L. Barabási, and P. Schiffer, What keeps sandcastles standing? Nature (London) **387**, 765 (1997).
[37] A. Groisman and E. Kaplan, An experimental study of cracking induced by desiccation, Europhys. Lett. **25**, 415 (1994).
[38] H. Shin and J. C. Santamarina, Fluid-driven fractures in uncemented sediments: Underlying particle-level processes, Earth Planet. Sci. Lett. **299**, 180 (2010).
[39] H. J. Cho, N. B. Lu, M. P. Howard, R. A. Adams, and S. S. Datta, Crack formation and self-closing in shrinkable, granular packings, Soft Matter (Weinheim, Ger.) **15**, 4689 (2019).
[40] B. Sandnes, H. A. Knudsen, K. J. Måløy, and E. G. Flekkøy, Labyrinth Patterns in Confined Granular-Fluid Systems, Phys. Rev. Lett. **99**, 038001 (2007).
[41] B. Sandnes, E. G. Flekkøy, H. A. Knudsen, K. J. Måløy, and H. See, Patterns and flow in frictional fluid dynamics, Nat. Commun. **2**, 288 (2011).
[42] A. Parmigiani, S. Faroughi, C. Huber, O. Bachmann, and Y. Su, Bubble accumulation and its role in the evolution of magma reservoirs in the upper crust, Nature (London) **532**, 492 (2016).
[43] R. Weinberger, Initiation and growth of cracks during desiccation of stratified muddy sediments, J. Struct. Geol. **21**, 379 (1999).
[44] B. Zhao, C. W. MacMinn, M. L. Szulczewski, J. A. Neufeld, H. E. Huppert, and R. Juanes, Interface pinning of immiscible gravity-exchange flows in porous media, Phys. Rev. E **87**, 023015 (2013).
[45] P.-G. de Gennes, F. Brochard-Wyart, and D. Quéré, *Capillarity and Wetting Phenomena: Drops, Bubbles, Pearls, Waves* (Springer, New York, 2004).
[46] R. Lenormand, C. Zarcone, and A. Sarr, Mechanisms of the displacement of one fluid by another in a network of capillary ducts, J. Fluid Mech. **135**, 337 (1983).
[47] W. B. Haines, Studies in the physical properties of soils. V. The hysteresis effect in capillary properties, and the modes of moisture redistribution associated therewith, J. Agric. Sci. **20**, 97 (1930).
[48] J. G. Roof, Snap-off of oil droplets in water-wet pores, Soc. Pet. Eng. J. **10**, 85 (1970).
[49] F. Moebius and D. Or, Interfacial jumps and pressure bursts during fluid displacement in interacting irregular capillaries, J. Colloid Interface Sci. **377**, 406 (2012).
[50] R. T. Armstrong and S. Berg, Interfacial velocities and capillary pressure gradients during Haines jumps, Phys. Rev. E **88**, 043010 (2013).
[51] S. Berg, H. Ott, S. A. Klapp, A. Schwing, R. Neiteler, N. Brussee, A. Makurat, L. Leu, F. Enzmann, J.-O. Schwarz, M. Kersten, S. Irvine, and M. Stampanoni, Real-time 3D imaging of Haines jumps in porous media flow, Proc. Natl. Acad. Sci. U.S.A. **110**, 3755 (2013).
[52] K. J. Måløy, L. Furuberg, J. Feder, and T. Jøssang, Dynamics of Slow Drainage in Porous Media, Phys. Rev. Lett. **68**, 2161 (1992).
[53] L. Furuberg, K. J. Måløy, and J. Feder, Intermittent behavior in slow drainage, Phys. Rev. E **53**, 966 (1996).
[54] R. Chandler, J. Koplik, K. Lerman, and J. F. Willemsen, Capillary displacement and percolation in porous media, J. Fluid Mech. **119**, 249 (1982).
[55] D. Wilkinson and J. Willemsen, Invasion percolation: A new form of percolation theory, J. Phys. A **16**, 3365 (1983).
[56] R. Lenormand and C. Zarcone, Invasion Percolation in an Etched Network: Measurement of a Fractal Dimension, Phys. Rev. Lett. **54**, 2226 (1985).
[57] R. Lenormand, E. Touboul, and C. Zarcone, Numerical models and experiments on immiscible displacements in porous media, J. Fluid Mech. **189**, 165 (1988).
[58] R. Lenormand, Liquids in porous media, J. Phys.: Condens. Matter **2**, SA79 (1990).
[59] L. Paterson, Diffusion-Limited Aggregation and Two-Fluid Displacements in Porous Media, Phys. Rev. Lett. **52**, 1621 (1984).

[60] K. J. Måløy, J. Feder, and T. Jøssang, Viscous Fingering Fractals in Porous Media, Phys. Rev. Lett. **55**, 2688 (1985).
[61] J.-D. Chen and D. Wilkinson, Pore-Scale Viscous Fingering in Porous Media, Phys. Rev. Lett. **55**, 1892 (1985).
[62] J.-D. Chen, Radial viscous fingering patterns in Hele-Shaw cells, Exp. Fluids **5**, 363 (1987).
[63] S. Bryant and M. J. Blunt, Prediction of relative permeability in simple porous media, Phys. Rev. A **46**, 2004 (1992).
[64] E. Aker, K. J. Måløy, and A. Hansen, Simulating temporal evolution of pressure in two-phase flow in porous media, Phys. Rev. E **58**, 2217 (1998).
[65] E. Aker, K. J. Måløy, A. Hansen, and G. G. Batrouni, A two-dimensional network simulator for two-phase flow in porous media, Transp. Porous Media **32**, 163 (1998).
[66] M. J. Blunt, Flow in porous media—Pore network models and multiphase flow, Curr. Opin. Colloid Interface Sci. **6**, 197 (2001).
[67] M. J. Blunt, M. D. Jackson, M. Piri, and P. H. Valvatne, Detailed physics, predictive capabilities and macroscopic consequences for pore-network models of multiphase flow, Adv. Water Resour. **25**, 1069 (2003).
[68] M. S. Al-Gharbi and M. J. Blunt, Dynamic network modeling of two-phase drainage in porous media, Phys. Rev. E **71**, 016308 (2005).
[69] V. Joekar-Niasar, S. M. Hassanizadeh, and H. K. Dahle, Non-equilibrium effects in capillarity and interfacial area in two-phase flow: Dynamic pore-network modelling, J. Fluid Mech. **655**, 38 (2010).
[70] V. Joekar-Niasar and S. M. Hassanizadeh, Analysis of fundamentals of two-phase flow in porous media using dynamic pore-network models: A review, Crit. Rev. Environ. Sci. Technol. **42**, 1895 (2012).
[71] M. A. Gjennestad, M. Vassvik, S. Kjelstrup, and A. Hansen, Stable and efficient time integration of a dynamic pore network model for two-phase flow in porous media, Front. Phys. **6**, 56 (2018).
[72] B. K. Primkulov, S. Talman, K. Khaleghi, A. Rangriz Shokri, R. Chalaturnyk, B. Zhao, C. W. MacMinn, and R. Juanes, Quasi-static fluid-fluid displacement in porous media: Invasion-percolation through a wetting transition, Phys. Rev. Fluids **3**, 104001 (2018).
[73] B. K. Primkulov, A. A. Pahlavan, X. Fu, B. Zhao, C. W. MacMinn, and R. Juanes, Signatures of fluid-fluid displacement in porous media: Wettability, patterns, and pressures, J. Fluid Mech. **875**, R4 (2019).
[74] H. T. Kennedy, E. O. Burja, and R. S. Boykin, An investigation of the effects of wettability on the recovery of oil by water flooding, J. Phys. Chem. **59**, 867 (1955).
[75] P. P. Jadhunandan and N. R. Morrow, Effect of wettability on waterflood recovery for crude-oil/brine/rock systems, SPE Reservoir Eng. **10**, 40 (1995).
[76] A. Seethepalli, B. Adibhatla, and K. K. Mohanty, Physicochemical interactions during surfactant flooding of fractured carbonate reservoirs, Soc. Pet. Eng. J. **9**, 411 (2004).
[77] N. Morrow and J. Buckley, Improved oil recovery by low salinity waterflooding, JPT, J. Pet. Technol. **63**, 106 (2011).
[78] G. Sharma and K. K. Mohanty, Wettability alteration in high-temperature and high-salinity carbonate reservoirs, Soc. Pet. Eng. J. **18**, 646 (2013).
[79] M. Alava, M. Dubé, and M. Rost, Imbibition in disordered media, Adv. Phys. **53**, 83 (2004).
[80] A. Hernández-Machado, J. Soriano, A. M. Lacasta, M. A. Rodriguez, L. Ramírez-Piscina, and J. Ortín, Interface roughening in Hele-Shaw flows with quenched disorder: Experimental and theoretical results, Europhys. Lett. **55**, 194 (2001).
[81] R. Planet, S. Santucci, and J. Ortín, Avalanches and Non-Gaussian Fluctuations of the Global Velocity of Imbibition Fronts, Phys. Rev. Lett. **102**, 094502 (2009).
[82] X. Clotet, J. Ortín, and S. Santucci, Disorder-Induced Capillary Bursts Control Intermittency in Slow Imbibition, Phys. Rev. Lett. **113**, 074501 (2014).
[83] M. Cieplak and M. O. Robbins, Dynamical Transition in Quasistatic Fluid Invasion in Porous Media, Phys. Rev. Lett. **60**, 2042 (1988).
[84] M. Cieplak and M. O. Robbins, Influence of contact angle on quasistatic fluid invasion of porous media, Phys. Rev. B **41**, 11508 (1990).

[85] P. E. Øren, S. Bakke, and O. J. Arntzen, Extending predictive capabilities to network models, Soc. Pet. Eng. J. **3**, 324 (1998).
[86] T. W. Patzek, Verification of a complete pore network simulator of drainage and imbibition, Soc. Pet. Eng. J. **6**, 144 (2001).
[87] P. H. Valvatne and M. J. Blunt, Predictive pore-scale modeling of two-phase flow in mixed wet media, Water Resour. Res. **40**, W07406 (2004).
[88] E. J. Spiteri, R. Juanes, M. J. Blunt, and F. M. Orr, Jr., A new model of trapping and relative permeability hysteresis for all wettability characteristics, Soc. Pet. Eng. J. **13**, 277 (2008).
[89] K. Singh, M. Jung, M. Brinkmann, and R. Seemann, Capillary-dominated fluid displacement in porous media, Annu. Rev. Fluid Mech. **51**, 429 (2019).
[90] M. Trojer, M. L. Szulczewski, and R. Juanes, Stabilizing Fluid-Fluid Displacements in Porous Media through Wettability Alteration, Phys. Rev. Appl. **3**, 054008 (2015).
[91] B. Zhao, C. W. MacMinn, and R. Juanes, Wettability control on multiphase flow in patterned microfluidics, Proc. Natl. Acad. Sci. U.S.A. **113**, 10251 (2016).
[92] R. Holtzman and E. Segre, Wettability Stabilizes Fluid Invasion into Porous Media via Nonlocal, Cooperative Pore Filling, Phys. Rev. Lett. **115**, 164501 (2015).
[93] B. Levaché, A. Azioune, M. Bourrel, V. Studer, and D. Bartolo, Engineering the surface properties of microfluidic stickers, Lab Chip **12**, 3028 (2012).
[94] B. K. Primkulov, A. A. Pahlavan, X. Fu, B. Zhao, C. W. MacMinn, and R. Juanes, Wettability and Lenormand's diagram (unpublished).
[95] B. Zhao, C. W. MacMinn, B. K. Primkulov, Y. Chen, A. J. Valocchi, J. Zhao, Q. Kang, K. Bruning, J. E. McClure, C. T. Miller, A. Fakhari, D. Bolster, T. Hiller, M. Brinkmann, L. Cueto-Felgueroso, D. A. Cogswell, R. Verma, M. Prodanović, J. Maes, S. Geiger *et al.*, Comprehensive comparison of pore-scale models for multiphase flow in porous media, Proc. Natl. Acad. Sci. U.S.A. **120**, 13799 (2019).
[96] F. M. Orr, L. E. Scriven, and A. P. Rivas, Pendular rings between solids: Meniscus properties and capillary force, J. Fluid Mech. **67**, 723 (1975).
[97] A. T. Skjeltorp and P. Meakin, Fracture in microsphere monolayers studied by experiment and computer simulation, Nature (London) **335**, 424 (1988).
[98] P. Meakin, Models for material failure and deformation, Science **252**, 226 (1991).
[99] J. Aizenberg, P. V. Braun, and P. Wiltzius, Patterned Colloidal Deposition Controlled by Electrostatic and Capillary Forces, Phys. Rev. Lett. **84**, 2997 (2000).
[100] M. Scheel, R. Seemann, M. Brinkmann, M. Di Michiel, A. Sheppard, B. Breidenbach, and S. Herminghaus, Morphological clues to wet granular pile stability, Nat. Mater. **7**, 189 (2008).
[101] J. A. Cartwright, Episodic basin-wide fluid expulsion from geopressured shale sequences in the North Sea basin, Geology **22**, 447 (1994).
[102] K. Andreassen, A. Hubbard, M. Winsborrow, H. Patton, S. Vadakkepuliyambatta, A. Plaza-Faverola, E. Gudlaugsson, P. Serov, A. Deryabin, R. Mattingsdal *et al.*, Massive blow-out craters formed by hydrate-controlled methane expulsion from the arctic seafloor, Science **356**, 948 (2017).
[103] A. E. Lobkovsky, B. Jensen, A. Kudrolli, and D. H. Rothman, Threshold phenomena in erosion driven by subsurface flow, J. Geophys. Res. **109**, F04010 (2004).
[104] D. M. Abrams, A. E. Lobkovsky, A. P. Petroff, K. M. Straub, B. McElroy, D. C. Mohrig, A. Kudrolli, and D. H. Rothman, Growth laws for channel networks incised by groundwater flow, Nat. Geosci. **2**, 193 (2009).
[105] P. J. van den Hoek, G. M. M. Hertogh, A. P. Kooijman, Ph. de Bree, C. J. Kenter, and E. Papamichos, A new concept of sand production prediction: Theory and laboratory experiments, SPE Drill. Completion **15**, 261 (2000).
[106] M. K. Hubbert and D. G. Willis, Mechanics of hydraulic fracturing, Pet. Trans. AIME **210**, 153 (1957).
[107] E. Detournay, Mechanics of hydraulic fractures, Annu. Rev. Fluid Mech. **48**, 311 (2016).
[108] H. Van Damme, F. Obrecht, P. Levitz, L. Gatineau, and C. Laroche, Fractal viscous fingering in clay slurries, Nature (London) **320**, 731 (1986).
[109] E. Lemaire, P. Levitz, G. Daccord, and H. Van Damme, From Viscous Fingering to Viscoelastic Fracturing in Colloidal Fluids, Phys. Rev. Lett. **67**, 2009 (1991).

[110] C. W. MacMinn, E. R. Dufresne, and J. S. Wettlaufer, Fluid-Driven Deformation of a Soft Granular Material, Phys. Rev. X **5**, 011020 (2015).
[111] A. K. Jain and R. Juanes, Preferential mode of gas invasion in sediments: Grain-scale mechanistic model of coupled multiphase fluid flow and sediment mechanics, J. Geophys. Res. **114**, B08101 (2009).
[112] R. Holtzman, M. L. Szulczewski, and R. Juanes, Capillary Fracturing in Granular Media, Phys. Rev. Lett. **108**, 264504 (2012).
[113] C. Peco, W. Chen, Y. Liu, M. M. Bandi, J. E. Dolbow, and E. Fried, Influence of surface tension in the surfactant-driven fracture of closely-packed particulate monolayers, Soft Matter **13**, 5832 (2017).
[114] W. S. Holbrook, H. Hoskins, W. T. Wood, R. A. Stephen, and D. Lizarralde, Methane hydrate and free gas on the Blake Ridge from vertical seismic profiling, Science **273**, 1840 (1996).
[115] J. R. Boles, J. F. Clark, I. Leifer, and L. Washburn, Temporal variation in natural methane seep rate due to tides, Coal Oil Point area, California, J. Geophys. Res. **106**, 27077 (2001).
[116] K. U. Heeschen, A. M. Trehu, R. W. Collier, E. Suess, and G. Rehder, Distribution and height of methane bubble plumes on the Cascadia Margin characterized by acoustic imaging, Geophys. Res. Lett. **30**, 1643 (2003).
[117] E. A. Solomon, M. Kastner, I. R. MacDonald, and I. Leifer, Considerable methane fluxes to the atmosphere from hydrocarbon seeps in the Gulf of Mexico, Nat. Geosci. **2**, 561 (2009).
[118] N. L. B. Bangs, M. J. Hornbach, and C. Berndt, The mechanics of intermittent methane venting at South Hydrate Ridge inferred from 4D seismic surveying, Earth Planet. Sci. Lett. **310**, 105 (2011).
[119] C. S. Martens and J. Val Klump, Biogeochemical cycling in an organic-rich coastal marine basin. 1. Methane sediment-water exchange processes, Geochim. Cosmochim. Acta **44**, 471 (1980).
[120] J. P. Chanton and C. S. Martens, Seasonal variations in ebullitive flux and carbon isotopic composition of methane in a tidal freshwater estuary, Global Biogeochem. Cycle **2**, 289 (1988).
[121] J. Greinert, D. F. McGinnis, L. Naudts, P. Linke, and M. De Batist, Atmospheric methane flux from bubbling seeps: Spatially extrapolated quantification from a Black Sea shelf area, J. Geophys. Res. **115**, C01002 (2010).
[122] C. Varadharajan, R. Hermosillo, and H. F. Hemond, A low-cost automated trap to measure bubbling gas fluxes, Limnol. Oceanogr.: Methods **8**, 363 (2010).
[123] B. P. Scandella, L. Pillsbury, T. Weber, C. Ruppel, H. Hemond, and R. Juanes, Ephemerality of discrete methane vents in lake sediments, Geophys. Res. Lett. **43**, 4374 (2016).
[124] T. Delsontro, D. F. McGinnis, S. Sobek, I. Ostrovsky, and B. Wehrli, Extreme methane emissions from a Swiss hydropower reservoir: Contribution from bubbling sediments, Environ. Sci. Technol. **44**, 2419 (2010).
[125] P. B. Flemings, X. Liu, and W. J. Winters, Critical pressure and multiphase flow in Blake Ridge gas hydrates, Geology **31**, 1057 (2003).
[126] X. Liu and P. B. Flemings, Passing gas through the hydrate stability zone at southern Hydrate Ridge, offshore Oregon, Earth Planet. Sci. Lett. **241**, 211 (2006).
[127] X.-Z. Kong, W. Kinzelbach, and F. Stauffer, Migration of air channels: An instability of air flow in mobile saturated porous media, Chem. Eng. Sci. **64**, 1528 (2009).
[128] X.-Z. Kong, W. Kinzelbach, and F. Stauffer, Morphodynamics during air injection into water-saturated movable spherical granulates, Chem. Eng. Sci. **65**, 4652 (2010).
[129] G. Varas, V. Vidal, and J.-C. Géminard, Morphology of air invasion in an immersed granular layer, Phys. Rev. E **83**, 061302 (2011).
[130] G. Varas, V. Vidal, and J.-C. Géminard, Venting dynamics of an immersed granular layer, Phys. Rev. E **83**, 011302 (2011).
[131] A. Islam, S. Chevalier, I. Ben Salem, Y. Bernabe, R. Juanes, and M. Sassi, Characterization of the crossover from capillary invasion to viscous fingering to fracturing during drainage in a vertical 2D porous medium, Int. J. Multiphase Flow **58**, 279 (2014).
[132] S. Lee, J. Lee, R. Le Mestre, F. Xu, and C. W. MacMinn, Migration, trapping, and venting of gas in a soft granular material, Phys. Rev. Fluids **5**, 084307 (2020).
[133] G. Varas, V. Vidal, and J.-C. Géminard, Dynamics of crater formations in immersed granular materials, Phys. Rev. E **79**, 021301 (2009).

[134] B. P. Scandella, K. Delwiche, H. Hemond, and R. Juanes, Persistence of bubble outlets in soft, methane-generating sediments, J. Geophys. Res. **122**, 1298 (2017).
[135] Z. Sun and J. C. Santamarina, Grain-displacive gas migration in fine-grained sediments, J. Geophys. Res. **124**, 2274 (2019).
[136] M. J. Dalbe and R. Juanes, Morphodynamics of Fluid–Fluid Displacement in Three-Dimensional Deformable Granular Media, Phys. Rev. Appl. **9**, 024028 (2018).
[137] J.-M. Konrad and R. Ayad, Desiccation of a sensitive clay: Field experimental observations, Can. Geotech. J. **34**, 929 (1997).
[138] L. Pauchard, V. Lazarus, B. Abou, K. Sekimoto, G. Aitken, and C. Lahanier, Craquelures dans les couches picturales des peintures d'art, Reflets Phys. **3**, 5 (2007).
[139] M. Leang, F. Giorgiutti-Dauphine, L.-T. Lee, and L. Pauchard, Crack opening: From colloidal systems to paintings, Soft Matter **13**, 5802 (2017).
[140] L. Goehring, A. Nakahara, T. Dutta, S. Kitsunezaki, and S. Tarafdar, *Desiccation Cracks and Their Patterns: Formation and Modelling in Science and Nature* (Wiley & Sons, New York, 2015).
[141] L. Xu, S. Davies, A. B. Schofield, and D. A. Weitz, Dynamics of Drying in 3D Porous Media, Phys. Rev. Lett. **101**, 094502 (2008).
[142] E. R. Dufresne, E. I. Corwin, N. A. Greenblatt, J. Ashmore, D. Y. Wang, A. D. Dinsmore, J. X. Cheng, X. S. Xie, J. W. Hutchinson, and D. A. Weitz, Flow and Fracture in Drying Nanoparticle Suspensions, Phys. Rev. Lett. **91**, 224501 (2003).
[143] L. Goehring, W. J. Clegg, and A. F. Routh, Plasticity and Fracture in Drying Colloidal Films, Phys. Rev. Lett. **110**, 024301 (2013).
[144] K. A. Shorlin, J. R. de Bruyn, M. Graham, and S. W. Morris, Development and geometry of isotropic and directional shrinkage-crack patterns, Phys. Rev. E **61**, 6950 (2000).
[145] T. Hornig, I. M. Sokolov, and A. Blumen, Patterns and scaling in surface fragmentation processes, Phys. Rev. E **54**, 4293 (1996).
[146] S. Kitsunezaki, Fracture patterns induced by desiccation in a thin layer, Phys. Rev. E **60**, 6449 (1999).
[147] K.-T. Leung and Z. Néda, Pattern Formation and Selection in Quasistatic Fracture, Phys. Rev. Lett. **85**, 662 (2000).
[148] H. Shin and J. C. Santamarina, Desiccation cracks in saturated fine-grained soils: Particle-level phenomena and effective-stress analysis, Geotechnique **61**, 961 (2011).
[149] T. Cajuhi, L. Sanavia, and L. De Lorenzis, Phase-field modeling of fracture in variably saturated porous media, Comp. Mech. **61**, 299 (2018).
[150] T. Hu, J. Guilleminot, and J. E. Dolbow, A phase-field model of fracture with frictionless contact and random fracture properties: Application to thin-film fracture and soil desiccation, Comput. Methods Appl. Mech. Eng. **368**, 113106 (2020).
[151] H. J. Cho and S. S. Datta, Scaling Law for Cracking in Shrinkable Granular Packings, Phys. Rev. Lett. **123**, 158004 (2019).
[152] P. G. Saffman and G. I. Taylor, The penetration of a fluid into a porous medium or Hele-Shaw cell containing a more viscous liquid, Proc. R. Soc. London, Ser. A **245**, 312 (1958).
[153] B. Sandnes, E.G. Flekkøy, and K. J. Måløy, Stick slip displacement of confined granular mixtures: Bubble expansion, Eur. Phys. J.: Spec. Top. **204**, 19 (2012).
[154] J. A. Eriksen, R. Toussaint, K. J. Måløy, E. Flekkøy, O. Galland, and B. Sandnes, Pattern formation of frictional fingers in a gravitational potential, Phys. Rev. Fluids **3**, 013801 (2018).
[155] R. Toussaint, G. Løvoll, Y. Méheust, K. J. Måløy, and J. Schmittbuhl, Influence of pore-scale disorder on viscous fingering during drainage, Europhys. Lett. **71**, 583 (2005).
[156] R. Holtzman and R. Juanes, Crossover from fingering to fracturing in deformable disordered media, Phys. Rev. E **82**, 046305 (2010).
[157] F. K. Eriksen, R. Toussaint, K.-J. Måløy, and E. G. Flekkøy, Invasion patterns during two-phase flow in deformable porous media, Front. Phys. **3**, 81 (2015).
[158] C. Chevalier, A. Lindner, M. Leroux, and E. Clement, The instability of slow, immiscible, viscous liquid-liquid displacements in permeable media, J. Non-Newton. Fluid Mech. **158**, 63 (2009).

[159] H. Huang, F. Zhang, P. Callahan, and J. Ayoub, Granular Fingering in Fluid Injection into Dense Granular Media in a Hele-Shaw Cell, Phys. Rev. Lett. **108**, 258001 (2012).
[160] M. Trojer, P. de Anna, and R. Juanes, Impact of wetting on fracturing of granular media (unpublished).
[161] Y. Meng, B. K. Primkulov, Z. Yang, C. Y. Kwok, and R. Juanes, Jamming transition and emergence of fracturing in wet granular media, Phys. Rev. Res. **2**, 022012(R) (2020).
[162] Itasca Consulting Group, *Inc., PFC2D, v3.1–Theory and Background* (ITASCA, Minneapolis, MN, 2004).
[163] P. A. Cundall and O. D. L. Strack, Discrete numerical model for granular assemblies, Geotechnique **29**, 47 (1979).
[164] T. S. Majmudar, M. Sperl, S. Luding, and R. P. Behringer, Jamming Transition in Granular Systems, Phys. Rev. Lett. **98**, 058001 (2007).
[165] C. Heussinger and J.-L. Barrat, Jamming Transition as Probed by Quasistatic Shear Flow, Phys. Rev. Lett. **102**, 218303 (2009).
[166] A. J. Liu and S. R. Nagel, Nonlinear dynamics: Jamming is not just cool any more, Nature (London) **396**, 21 (1998).
[167] M. Moura, K. J. Måløy, and R. Toussaint, Critical behavior in porous media, Europhys. Lett. **118**, 14004 (2017).
[168] C. Odier, B. Levaché, E. Santanach-Carreras, and D. Bartolo, Forced Imbibition in Porous Media: A Fourfold Scenario, Phys. Rev. Lett. **119**, 208005 (2017).
[169] M. Saadatfar, A. P. Sheppard, T. J. Senden, and A. J. Kabla, Mapping forces in a 3D elastic assembly of grains, J. Mech. Phys. Solids **60**, 55 (2012).
[170] N. Brodu, J. A. Dijksman, and R. P. Behringer, Spanning the scales of granular materials through microscopic force imaging, Nat. Commun. **6**, 6361 (2015).
[171] R. C. Hurley, S. A. Hall, J. E. Andrade, and J. Wright, Quantifying Interparticle Forces and Heterogeneity in 3D Granular Materials, Phys. Rev. Lett. **117**, 098005 (2016).
[172] M. Frocht, *Photoelasticity* (Wiley & Sons, New York, 1941).
[173] T. S. Majmudar and R. P. Behringer, Contact force measurements and stress-induced anisotropy in granular materials, Nature (London) **435**, 1079 (2005).
[174] K. E. Daniels, J. E. Kollmer, and J. G. Puckett, Photoelastic force measurements in granular materials, Rev. Sci. Instrum. **88**, 051808 (2017).
[175] N. Iikawa, M. M. Bandi, and H. Katsuragi, Sensitivity of Granular Force Chain Orientation to Disorder-Induced Metastable Relaxation, Phys. Rev. Lett. **116**, 128001 (2016).
[176] S. Lherminier, R. Planet, G. Simon, L. Vanel, and O. Ramos, Revealing the Structure of a Granular Medium through Ballistic Sound Propagation, Phys. Rev. Lett. **113**, 098001 (2014).
[177] S. Lherminier, R. Planet, V. L. Vehel, G. Simon, L. Vanel, K. J. Måløy, and O. Ramos, Continuously Sheared Granular Matter Reproduces in Detail Seismicity Laws, Phys. Rev. Lett. **122**, 218501 (2019).
[178] A. L. Handwerger, A. W. Rempel, R. M. Skarbek, J. J. Roering, and G. E. Hilley, Rate-weakening friction characterizes both slow sliding and catastrophic failure of landslides, Proc. Natl. Acad. Sci. U.S.A. **113**, 10281 (2016).
[179] J. Palmer, Creeping catastrophes—Studies of slow landslides could unmask the mechanics of a worldwide scourge, Nature (London) **548**, 384 (2017).
[180] C. H. Scholz, Earthquakes and friction laws, Nature (London) **391**, 37 (1998).
[181] C. H. Scholz, *The Mechanics of Earthquakes and Faulting*, 3rd ed. (Cambridge University, Cambridge, England, 2019).
[182] Y. Jiang, G. Wang, and T. Kamai, Acoustic emission signature of mechanical failure: Iinsights from ring-shear friction experiments on granular materials, Geophys. Res. Lett. **44**, 2782 (2017).
[183] M. J. Ikari, D. M. Saffer, and C. Marone, Frictional and hydrologic properties of clay-rich fault gouge, J. Geophys. Res. **114**, B05409 (2009).
[184] M. Sawai, A. R. Niemeijer, O. Plümper, T. Hirose, and C. J. Spiers, Nucleation of frictional instability caused by fluid pressurization in subducted blueschist, Geophys. Res. Lett. **43**, 2543 (2016).
[185] M. M. Scuderi and C. Collettini, The role of fluid pressure in induced vs. triggered seismicity: Insights from rock deformation experiments on carbonates, Sci. Rep. **6**, 24852 (2016).

[186] M. M. Scuderi, C. Collettini, and C. Marone, Frictional stability and earthquake triggering during fluid pressure stimulation of an experimental fault, Earth Planet. Sci. Lett. **477**, 84 (2017).
[187] F. Cappa, M. M. Scuderi, C. Collettini, Y. Guglielmi, and J.-P. Avouac, Stabilization of fault slip by fluid injection in the laboratory and in situ, Sci. Adv. **5**, eaau4065 (2019).
[188] T. Xing, W. Zhu, M. French, and B. Belzer, Stabilizing effect of high pore fluid pressure on slip behaviors of gouge-bearing faults, J. Geophys. Res. **124**, 9526 (2019).
[189] M. F. Linker and J. H. Dieterich, Effects of variable normal stress on rock friction: Observations and constitutive equations, J. Geophys. Res. **97**, 4923 (1992).
[190] C. Marone, C. B. Raleigh, and C. H. Scholz, Frictional behavior and constitutive modeling of simulated fault gouge, J. Geophys. Res. **95**, 7007 (1990).
[191] Y. Guglielmi, F. Cappa, J.-P. Avouac, P. Henry, and D. Elsworth, Seismicity triggered by fluid injection-induced aseismic slip, Science **348**, 1224 (2015).
[192] https://commons.wikimedia.org/wiki/File:Ultimate_Sand_Castle.jpg.